arXiv:1205.6345v1 [physics.acc-ph] 29 May 2012

DEUTSCHES ELEKTRONEN-SYNCHROTRON

Ein Forschungszentrum der Helmholtz-Gemeinschaft

DESY 12-082

May 2012

Conceptual design of an undulator system for a dedicated bio-imaging beamline at the European X-ray FEL

Gianluca Geloni,
European XFEL GmbH, Hamburg

Vitali Kocharyan and Evgeni Saldin
Deutsches Elektronen-Synchrotron DESY, Hamburg

ISSN 0418-9833

NOTKESTRASSE 85 - 22607 HAMBURG

Conceptual design of an undulator system for a dedicated bio-imaging beamline at the European X-ray FEL

Gianluca Geloni, [a,1] Vitali Kocharyan [b] and Evgeni Saldin [b]

[a] *European XFEL GmbH, Hamburg, Germany*
[b] *Deutsches Elektronen-Synchrotron (DESY), Hamburg, Germany*

Abstract

We describe a future possible upgrade of the European XFEL consisting in the construction of an undulator beamline dedicated to life science experiments. The availability of free undulator tunnels at the European XFEL facility offers a unique opportunity to build a beamline optimized for coherent diffraction imaging of complex molecules, like proteins and other biologically interesting structures. Crucial parameters for such bio-imaging beamline are photon energy range, peak power, and pulse duration. Key component of the setup is the undulator source. The peak power is maximized in the photon energy range between 3 keV and 13 keV by the use of a very efficient combination of self-seeding, fresh bunch and tapered undulator techniques. The unique combination of ultra-high peak power of 1 TW in the entire energy range, and ultrashort pulse duration tunable from 2 fs to 10 fs, would allow for single shot coherent imaging of protein molecules with size larger than 10 nm. Also, the new beamline would enable imaging of large biological structures in the water window, between 0.3 keV and 0.4 keV. In order to make use of standardized components, at present we favor the use of SASE3-type undulator segments. The number segments, 40, is determined by the tapered length for the design output power of 1 TW. The present plan assumes the use of a nominal electron bunch with charge of 0.1 nC. Experiments will be performed without interference with the other three undulator beamlines. Therefore, the total amount of scheduled beam time per year is expected to be up to 4000 hours.

[1] Corresponding Author. E-mail address: gianluca.geloni@xfel.eu

1 Introduction

Structural biology aims at the understanding of the biological function of proteins by studying their three-dimensional structure. The major method for determining such macromolecular three-dimensional structure is X-ray crystallography [1, 2]. Requirements on the crystal samples set limits to structural studies of biological systems with atomic resolution. In fact, many molecules fail to form crystals. The development of XFELs promises to open up new areas in life science by allowing structure determination without the need for crystallization. In fact, as suggested in [3], sufficiently short and intense pulses from X-ray lasers may allow for the imaging of single protein molecules.

This article describes a possible future upgrade of the European XFEL. We present a study for a dedicated beamline for single-biomolecular imaging. The main idea is to use one of the free undulator tunnels of the European XFEL for providing the user community with the three SASE1, SASE2 and SASE3 lines, with the addition of a fourth beamline where the combination of 1 TW peak power in the energy range between 3 keV and 13 keV, and tunability of the pulse duration from 2 fs to 10 fs will provide significantly better conditions for single shot coherent imaging of protein molecules than at other XFEL facilities.

The European XFEL equipped with a dedicated bio-imaging beamline represents a development half way in between a proof-of-principle and a fully dedicated bio-imaging XFEL facility with high-rate of protein structure determination. The main advantage of the new beamline is the operation point at 1 TW with 2 fs-5 fs long pulses in the particular energy range between 3 keV and 5 keV, where the diffraction signal is strong. Operation at 1 TW in this peculiar energy range will not be accessible to other XFEL facilities at least until the end of the next decade. These characteristics would enable new exciting possibilities for coherent imaging of protein molecules with size larger than 10 nm.

2 Scientific aims

Understanding the biological function of molecules such as proteins, requires the knowledge of their atomic structure. Today, X-ray crystallography is a major technique to determine the atomic structure of proteins. However, there is still a serious limiting factor: in fact, many molecules fail to form crystals, which prevents X-ray protein crystallography from fully realizing its potential [1, 2]. In particular, it is known that about 40% of

biomolecules, in particular membrane proteins, do not crystallize. Hence, the scattering signal is too small to be useful. Increasing the number of photons in the pulse without decreasing its duration does not help, since radiation damage severely limits structural studies of single biomolecules.

The development of XFELs promises to open up new area in life science by allowing structure determination of difficult-to-crystallize proteins. Single biomolecules are injected into a pulsed X-ray beam. Imaging of a single biomolecule can then be performed through coherent diffraction experiments [3]. The elastically scattered photons are recorded by a detector array placed downstream. The scattered pattern contains information in the reciprocal space, from which the object may be reconstructed [4]. The advantage of using an XFEL source is in the ultrashort time scale of the XFEL pulse. The scattering pattern can be recorded before the molecule is destroyed. This effect is known as diffraction before destruction [5]. Simulations and experiments suggest that radiation damage will not significantly disrupts the initial positions of atoms in the first few femtoseconds of exposure and that the object may be reconstructed [6].

Focusing optics is used to closely match the size of the X-ray beam to the size of the sample, and to maximize the signal level. The FWHM focal spot size should be about $5-10$ times larger than the sample size. For example, a spot size of 100 nm is good for sample sizes smaller than 10 nm. The total number of different proteins smaller than 10 nm is about 10^5. Structure determination of many of these (about 80000) has been successfully performed [7]. The largest number of biologically interesting structures are in the size range between 10 nm and 600 nm. The total number of different structures of this kind is over 10^9. Only very few of these structures have been determined [8].

Let us estimate the minimum number of required photons per XFEL pulse for successful imaging of single biomolecules. An incident photon flux of 10^{21} photons/mm^2 is sufficient for obtaining a reasonably good image of a protein molecule like a lysozyme (14 kD) with a size of about 6 nm at photon energy of 12 keV [9]. The "diffraction-before-destruction" method requires a pulse duration shorter than 10 fs. The number of photons per pulse required for a typical experiments is about $2 \cdot 10^{12}$. An important problem parameter is the number of scattered photons per effective pixel, which is proportional to λ^2, where λ is the radiation wavelength. As a result, lower photon energies result in a stronger diffraction signal. However, a decrease in the photon energy limits the resolution. A balance may be reached in the photon energy range between 3 keV and 5 keV.

The main application of the beamline proposed in this work is for single shot imaging of individual protein molecules. It will provide coherent X-

ray radiation with properties superior to the existing and planned XFEL sources. The X-ray beam will be delivered in ultrashort pulses with a duration between 2 fs and 10 fs, with 1 TW peak power, and within a very wide photon energy range between 3 keV and 13 keV, which covers the K-edge energies from sulfur to selenium. The beamline is also designed to provide photon energies down to water window at 0.3 keV. We believe that our developments will open exciting possibilities for structure determination of protein molecules with size larger than 10 nm and in the 3 keV - 5 keV photon energy range of operation.

3 Basic concept of the bio-imaging beamline

For the realization of the bio-imaging beamline we propose to use the same undulator technology optimized for the generation of soft X-rays at the European XFEL. The installation and commissioning of the new beamline can take place gradually. In the beginning, the new beamline would just extend the soft X-ray (SASE3) beamline and take advantage of the long XTD4 tunnel. An additional undulator composed by 19 cells would be added into the 300 m-long XTD4 tunnel. This undulator would extend the existing SASE3 line, composed by 21 cells, and have the same period of SASE3, in order to obtain a total cell number of 40. With this, SASE3 would be de facto converted into a bio-imaging beamline. Then, a new soft X-ray beamline, identical to the SASE3 baseline, could be installed in the free 150 m-long XTD3 tunnel.

The combination of self-seeding and tapered undulator techniques would allow to meet the design output peak power of 1 TW. The bio-imaging beamline would be equipped with two different self-seeding setup, one to provide monochromatization in the soft X-ray range, between 0.3 keV and 1.7 keV, and one to provide monochromatization in the hard X-ray range between 8 keV and 13 keV. A border region exists between the soft and the hard X-ray range. In fact, the X-ray optics for the self-seeding scheme adopted in one range is not suitable for the other, and vice versa. Self-seeding schemes with crystal monochromators work above 7 keV, where diamond crystals can be used. Crystals with the right lattice parameters and with sufficiently narrow linewidth are difficult to be obtained. Diffraction gratings with single metal layer coating (Au, Pt) have good first order efficiency at grazing angles up to 2 keV, but at higher energies their throughput is usually too low. Such gratings are conceived for the soft- X-ray self-seeding setup at the LCLS. A combination of these two self-seeding setups with a tunable gap, 40 cells-long undulator would allow to meet the design goal of 1 TW for photon energies ranging between 0.3 keV and 1.7 keV, and between 8 keV and 13 keV.

However, the users of the bio-imaging beamline mainly wish to investigate their samples in the energy range between 3 keV and 5 keV, where the diffraction signal is strong. Finding a solution suitable for this spectral range is major challenge for self-seeding designers. A promising approach in this direction consists in using a fresh bunch technique in combination with self-seeding and tapering techniques. We will show how installation of an additional chicane behind the soft X-ray self-seeding setup enables an output peak power around 1 TW for photon energy ranges between 3 keV and 5 keV. The combination self-seeding, fresh bunch and tapered techniques has the advantage that it does not need any significant change in the grating monochromator design proposed by the LCLS crew, which is still under active investigation [10, 11, 12]. It should be noted that the duration of the X-ray pulse is important for bio-imaging experiments. In particular, for energies smaller than 5 keV, the pulse duration should be shorter than 5 fs. We will show how the pulse duration can be tuned within 2 fs and 10 fs, still operating with nominal electron bunch distributions.

The two design electron energies for the new beamline will be 10 GeV and 17 GeV, at a design charge of 0.1 nC. When the bio-imaging beamline will run at 10 GeV electron energy, it will be necessary to run all the FEL lines at the same energy, although this may not be the preferred mode of operation for SASE1 and SASE2 users. However, this electron energy is still one of the nominal electron energies for the European XFEL, and is compatible with the operation of SASE1 and SASE2 in the X-ray energy range up to 12 keV.

After conversion of the SASE3 beamline as described in this report there will be several future upgrade options for a dedicated bio-imaging beamline. To avoid interference with other beamlines, the photon energy range of the self-seeding setup with grating monochromator can be extended up to 5 keV, and the minimal design electron energy can be increased up to 14 GeV. A promising approach in this direction consists in using diffraction gratings with very shallow groove depths, capable of working at very small angles of incidence. Recently, a holographic laminar grating has been realized and characterized in the energy range between 3 keV and 5 keV at the incidence angle of 0.5 degree, showing up to 10% efficiency [13].

3.1 Setup description

Self-seeding is a promising approach to significantly narrow the SASE bandwidth and to produce nearly transform-limited X-ray pulses [14]-[30]. In its simplest configuration the self-seeding setup in the hard X-ray regime consists of two undulators separated by photon monochromator and an electron bypass beamline, typically a 4-dipole chicane. The two undulators are res-

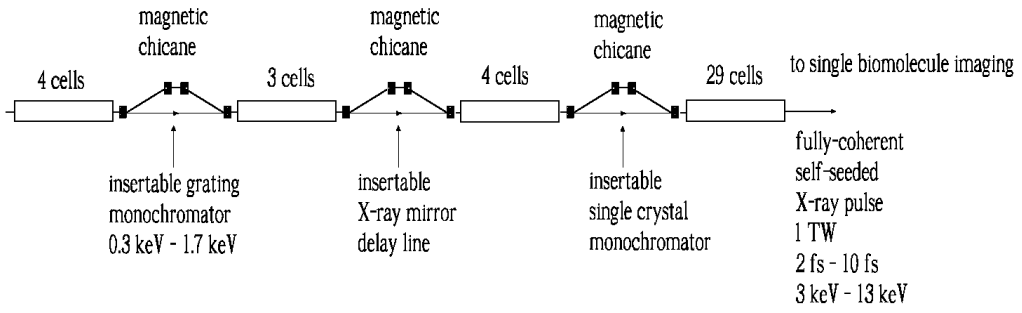

Fig. 1. Design of the undulator system for the bio-imaging beamline. The method exploits a combination of self-seeding, fresh bunch, and undulator tapering technique. Each magnetic chicane accomplishes three tasks by itself. It creates an offset for monochromator or X-ray mirror delay line installation, it removes the electron microbunching produced in the upstream undulator, and it acts as a magnetic delay line.

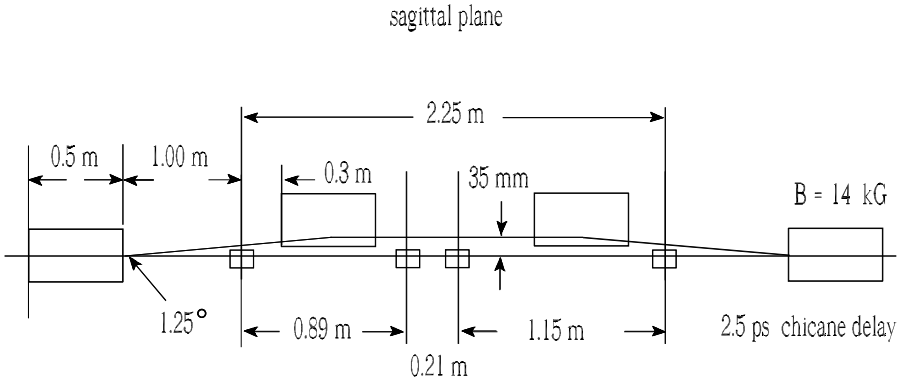

Fig. 2. Plan view of the self-seeding setup with compact grating monochromator originally proposed at SLAC [10, 11].

onant at the same radiation wavelength. The SASE radiation generated by the first undulator passes through the narrow-band monochromator, thus generating a transform-limited pulse, which is then used as a coherent seed in the second undulator. Chromatic dispersion effects in the bypass chicane smear out the microbunching in the electron bunch produced by the SASE lasing in the first undulator. Electrons and monochromatized photon beam are recombined at the entrance of the second undulator, and the radiation is amplified by the electron bunch in the second undulator, until saturation is reached. The required seed power at the beginning of the second undulator

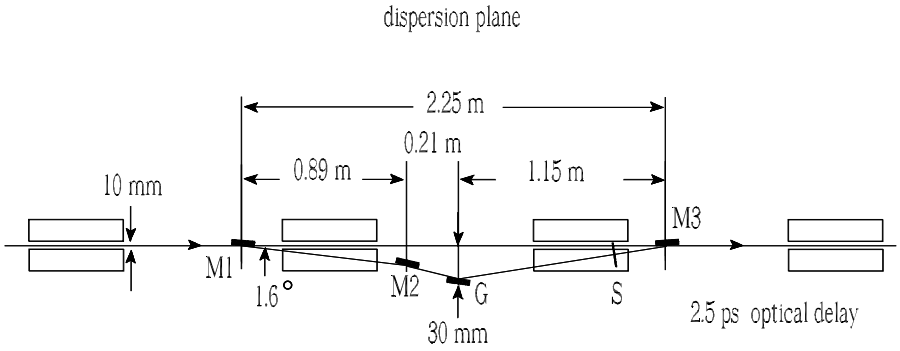

Fig. 3. Elevation view of the self-seeding setup with compact grating monochromator originally proposed at SLAC [10, 11].

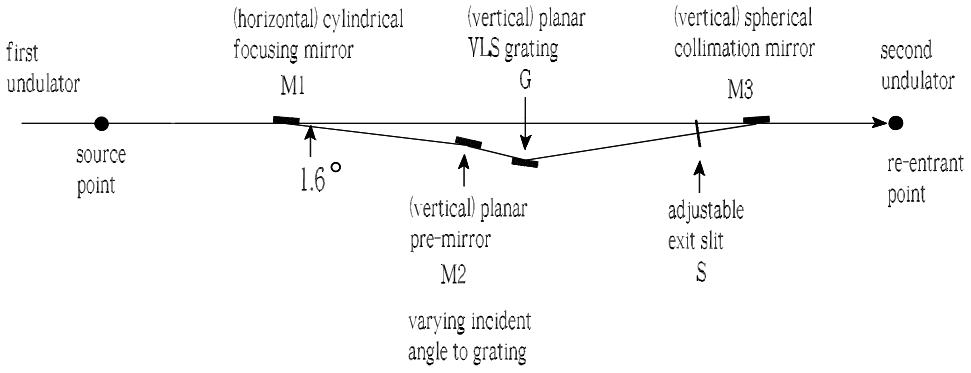

Fig. 4. Optics for the compact grating monochromator originally proposed at SLAC [10, 11] for the soft X-ray self-seeding setup.

must dominate over the shot noise power within the gain bandpass, which is order of a few kW.

Despite the unprecedented increase in peak power of the X-ray pulses for SASE X-ray FELs (see e.g. [31]), some applications, including single biomolecule imaging, require still higher photon flux. The most promising way to extract more FEL power than that at saturation is by tapering the magnetic field of the undulator [32]-[39]. Also, a significant increase in power is achievable by starting the FEL process from a monochromatic seed rather than from noise [25]-[30]. Tapering consists in a slow reduction of the field strength of the undulator in order to preserve the resonance wavelength, while the kinetic energy of the electrons decreases due to the FEL process. The undulator taper could be simply implemented as a step from

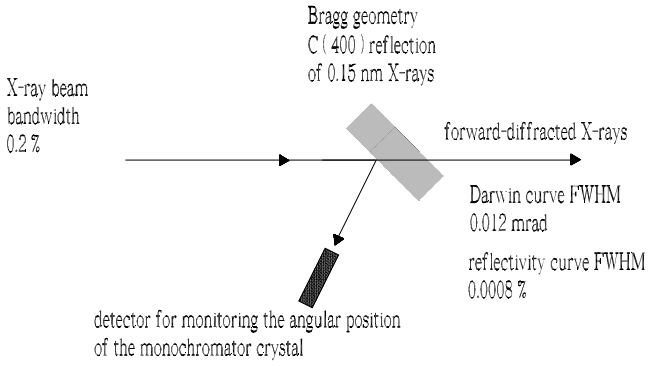

Fig. 5. X-ray optics for compact crystal monochromator originally proposed in [27] for a hard X-ray self-seeding setup.

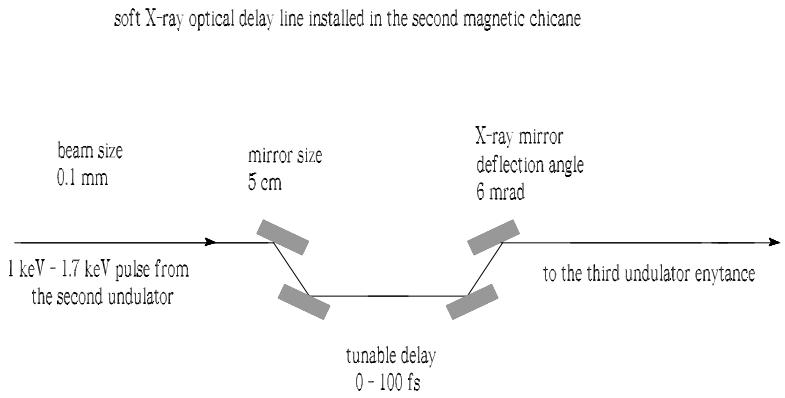

Fig. 6. X-ray optical system for delaying the soft X-ray pulse with respect to the electron bunch. The X-ray optical system can be installed within the second magnetic chicane of the fresh bunch setup.

one undulator segment to the next. The magnetic field tapering is provided by changing the undulator gap.

The proposed setup is not simple as discussed above and is composed of four undulators separated by three magnetic chicanes as shown in Fig. 1. These undulators consist of 4, 3, 4 and 29 undulator cells, respectively. Each magnetic chicane is compact enough to fit one undulator segment. The installation of chicanes does not perturb the undulator focusing system. The implementation of the self-seeding scheme for soft X-ray and hard X-ray would exploit the first and the third magnetic chicane, respectively. Both self-seeding setups should be compact enough to fit one undulator module.

For soft X-ray self-seeding, the monochromator usually consists of a grating [14]. Recently, a very compact soft X-ray self-seeding scheme has appeared, based on a grating monochromator [10, 11]. The proposed monochromator is composed of only three mirrors and a rotational VLS grating. It is equipped with an exit slit only. A preliminary design of the grating monochromator adopts a constant focal-point mode in order to fix the slit location. The delay of the photons is about 2.5 ps. The monochromator is continuously tunable in the photon energy range between 0.3 keV and 1.7 keV. The resolution is about 5000. The transmission of the monochromator beamline is close to 10%. The magnetic chicane delays the electron electron bunch accordingly, so that the photon beam passing through the monochromator system recombines with the same electron bunch. The chicane provides a dispersion strength of about 2 mm in order to match the optical delay and also smears out the SASE microbunching generated in the first 4 cells of the undulator. The final design is under active investigations, and is subject to many changes [12]. In [40] we studied the performance of the above-described scheme for the European XFEL upgrade. For bio-imaging beamline we adopt the same design as in [10, 11]. The layout of the bypass and of the monochromator optics is schematically shown in Fig. 2, Fig. 3 and Fig. 4.

For hard X-ray self-seeding, a monochromator usually consists of crystals in the Bragg geometry. A conventional 4-crystal, fixed exit monochromator introduces optical delay of, at least, a few millimeters, which has to be compensated with the introduction of an electron bypass longer than one undulator module. To avoid this difficulty, a simpler self-seeding scheme was proposed in [27], which uses the transmitted X-ray beam from the single crystal to seed the same electron bunch, Fig. 5. Here we propose to use a diamond crystal with a thickness of 0.1 mm. For a symmetric C(400) Bragg reflection, it will be possible to cover the photon energy range from 8 keV to 13 keV.

One of the main technical problems to provide bio-imaging capabilities in 3 keV - 5 keV photon energy range is the extension of the self-seeding grating monochromator design from 2 keV up to 5 keV. Here we propose a method to get around this obstacle. Our solution is based in essence on the fresh bunch technique [28] and exploits the above described conservative design of self-seeding setup based on a grating monochromator. The hardware requirement is minimal, and in order to implement a fresh bunch technique it is sufficient to install an additional magnetic chicane at a special position behind the soft X-ray self-seeding setup. The function of this second chicane is both to smear out the electron bunch microbunching, and to delay the electron bunch with respect to the monochromatic soft X-ray pulse produced in the second undulator. In this way, only half of the electron bunch is seeded, and saturates in the third undulator. Finally, the second half of the electron

bunch, which remains unspoiled, is seeded by the third harmonic of the monochromatic radiation pulse generated in the third undulator, which is also monochromatic. The final delay of the electron bunch with respect to the seed radiation pulse can be obtained with a third, hard X-ray self-seeding magnetic chicane, which in this mode of operation is simply used to provide magnetic delay. The monochromatic third harmonic radiation pulse used as seed for the unperturbed part of the electron bunch is in the GW power level, and the combination of self-seeding and fresh bunch technique is extremely insensitive to non-ideal effects. The final undulator, composed by 29 cells, is tuned to the third harmonic frequency, and is simply used to amplify the X-ray pulse up to 1 TW output power level.

It should be noted that the delay of the radiation pulse with respect to the electron bunch in the second and in the third chicane has a different sign. The solution to this problem is to install a mirror chicane within the second magnetic chicane, as shown in Fig. 6. The function of the mirror chicane is to delay the radiation in the range between 1 keV and 1.7 keV relatively to the electron bunch. The glancing angle of the mirrors is as small as 3 mrad. At the undulator location, the transverse size of the photon beam is smaller than 0.1 mm, meaning that the mirror length would be just about 5 cm. The single-shot mode of operation will relax the heat-loading issues. The mirror chicane can be built in such a way to obtain a delay of the radiation pulse of about 23 μm. This is enough to compensate a bunch delay of about 20 μm from the magnetic chicane, and to provide any desired shift in the range between 0 μm and 3 μm. Note that for the European XFEL parameters, 1 nm microbunching is washed out with a weak dispersive strength corresponding to an R_{56} in the order of ten microns. The dispersive strength of the proposed magnetic chicane is more than sufficient to this purpose. Thus, the combination of magnetic chicane and mirror chicane removes the electron microbunching produced in the second undulator and acts as a tunable delay line within 0 μm and 3 μm with the required choice of delay sign.

3.2 Generation of TW pulses in the 0.3 keV - 1.7 keV photon energy range

The four-undulator configuration in Fig. 1 can be naturally taken advantage of at different photon energies ranging from soft to hard X-rays. Fig. 7 shows the basic setup for the high-power mode of operation in the soft X-ray wavelength range. The second and the third chicanes are not used for such regime, and must be switched off. After the first undulator (4 cells-long) and the grating monochromator, the output undulator follows. The first section of the output undulator (consisting of second and third undulator) is composed by 7 untapered cells , while tapering is implemented in the

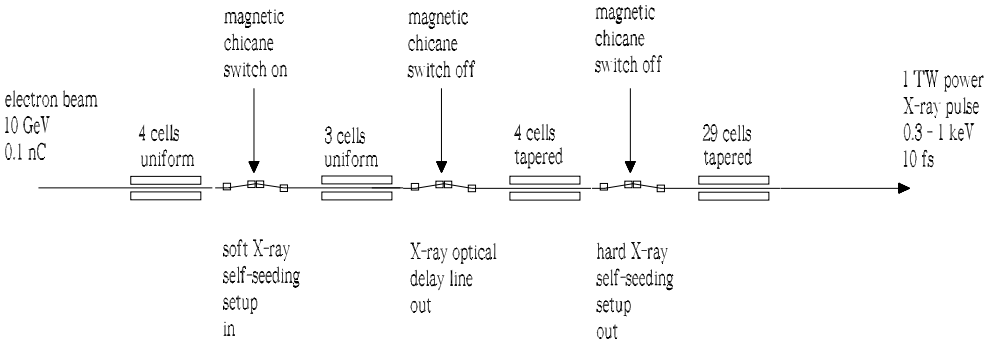

Fig. 7. Design of the undulator system for 1 TW power mode of operation in the soft X-ray photon energy range. The method exploits a combination of self-seeding scheme with grating monochromator and an undulator tapering technique.

fourth undulator. The monochromatic seed is exponentially amplified by passing through the first untapered section of the output undulator. This section is long enough to allow for saturation, and yields an output power of about 100 GW. Such monochromatic FEL output is finally enhanced up to 1 TW in the second output-undulator section, by tapering the undulator parameter over the last cells after saturation. Under the constraints imposed by undulator and chicane parameters it is only possible to operate at an electron beam energy of 10 GeV. The setup was optimized based on results of start-to-end simulations for a nominal electron beam with 0.1 nC charge. Results were presented in [40], where we studied the performance of this scheme for the SASE3 upgrade.

3.3 Generation of TW pulses in the 3 keV - 5 keV photon energy range

Fig. 8 shows the basic setup for high power mode of operation in the most preferable photon energy range for single biomolecule imaging. All three chicanes are used for such regime, and must be switched on. The third chicane is used as a magnetic delay only, and the crystal must be removed from the light path. We propose to perform monochromatization at photon energies ranging between 1 keV and 1.7 keV with the help of a grating monochromator, and to amplify the seed in the second undulator up to the power level of 0.2 GW. The second chicane smears out the electron microbunching and delays the monochromatic soft X-ray pulse of 2 μm with respect to the electron bunch. In this way, half of the electron bunch is seeded and saturates in the third undulator up to 40 GW, Fig. 9. At saturation, the electron beam generates considerable monochromatic radiation at the third

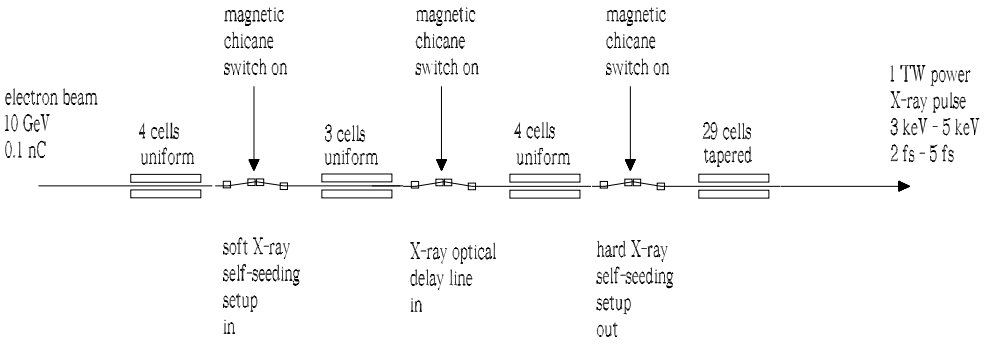

Fig. 8. Design of the undulator system for 1 TW power mode of operation in the 3 keV - 5 keV photon energy range. The method exploits a combination of self--seeding scheme with grating monochromator, fresh bunch and undulator tapering techniques.

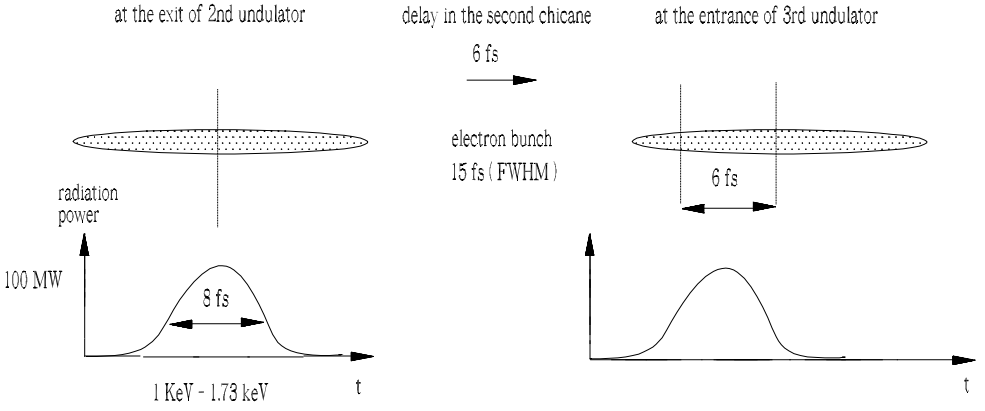

Fig. 9. Principle of the fresh bunch technique for the high power mode of operation in the photon energy range between 3 keV and 5 keV. The second chicane smears out the electron microbunching and delays the monochromatic soft X-ray pulse with respect to the electron bunch of 6 fs. In this way, half of of the electron bunch is seeded and saturates in the third undulator.

harmonic in the GW power level. The third magnetic chicane smears out the electron microbunching and delays the electron bunch with respect to the radiation of 2 μm. Thus, the unspoiled part of the electron bunch is seeded by the GW-level monochromatic pulse at the third harmonic frequency, Fig. 10. The fourth, 29 cells-long undulator is tuned to the third harmonic frequency (between 3 keV and 5 keV), and is used to amplify the radiation pulse up to 1 TW. The additional advantage of the proposed setup for bio-imaging is the tunability of the output pulse duration, which is obtained by

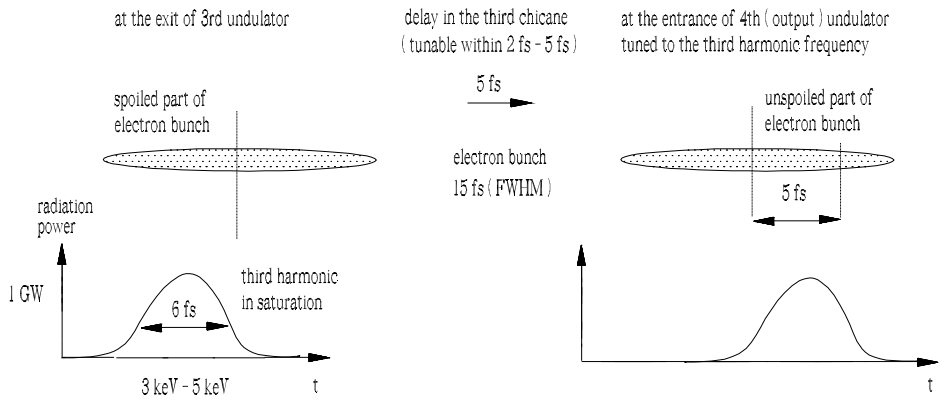

Fig. 10. Principle of the fresh bunch technique for the high power mode of operation in the photon energy range between 3 keV and 5 keV. The third magnetic chicane smears out the electron microbunching and delays the electron bunch with respect to the radiation pulse. The unspoiled part of electron bunch is seeded by a GW level monochromatic pulse at third harmonic frequency. Tunability of the output pulse duration can be easily obtained by tuning the magnetic delay of the third chicane.

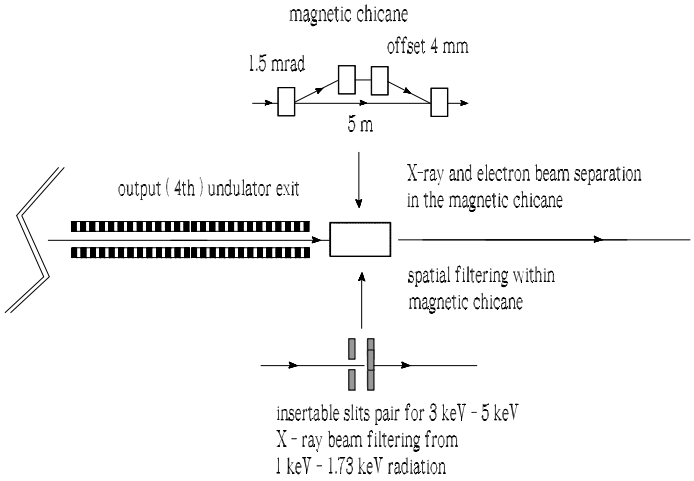

Fig. 11. Schematics of a background filtering setup downstream of the extended SASE3 undulator. The scheme for spatial filtering will make use of a short magnetic chicane immediately behind the exit of the output undulator, so that the electron beam bypasses the slits. Vertical and horizontal slits will positioned at 70 m (Phase one) or 200 m (Phase two) downstream of the third undulator, where the background radiation (between 1 keV and 1.73 keV) is characterized by a spot size ten times larger than that of the main X-ray beam (between 3 keV and 5 keV).

tuning the magnetic delay of the third chicane. Simulations show that the X-ray pulse duration can be tuned from 2 fs to 5 fs. The production of such pulses is of great importance when it comes to single biomolecule imaging experiments.

The soft X-ray background can be easily eliminated by using a spatial window positioned downstream of the fourth undulator exit, Fig. 11. Since the soft X-ray radiation has an angular divergence of about 0.02 mrad FWHM, and the slits are positioned more than 100 m downstream of the third undulator, the background has much larger spot size compared with the 3 keV - 5 keV radiation spot size, which is about 0.1 mm at the exit of the fourth undulator. Therefore, the background radiation power can be diminished of more than two orders of magnitude without any perturbations of the main pulse.

Under the constraints imposed by the soft X-ray self-seeding setup, it is only possible to operate at an electron beam energy of 10 GeV. The setup was optimized based on results of start-to-end simulations for a nominal electron bunch with a charge of 0.1 nC. Results are presented in Section 4. The proposed undulator setup uses the electron beam coming from the SASE1 undulator. We assume that SASE1 operates at the photon energy of 12 keV, and that the FEL process is switched off for one single dedicated electron bunch within each macropulse train. A method to control the FEL amplification process is based on betatron switcher described in [41, 42]. Due to quantum energy fluctuations in the SASE1 undulator, and to wakefields in the SASE1 undulator pipe, the energy spread and the energy chirp of the electron bunch at the entrance of the bio-imaging beamline significantly increases compared with the same parameters at the entrance of the SASE1 undulator. The dispersion strength of the first chicane has been taken account from the viewpoint of the electron beam dynamics, because it disturbs the electron beam distribution. The other two chicanes have tenfold smaller dispersion strength compared with first one. The electron beam was tracked through the first chicane using the code Elegant [43]. The electron beam distortions complicate the simulation procedure. However, simulations show (see Section 4) that the proposed setup is not significantly affected by perturbations of the electron phase space distribution, and yields about the same performance as in the case for an electron beam without chicane transformation (see below).

Finally, the design of the grating monochromator for the soft X-ray self-seeding scheme is under active investigation. For example, a more compact grating monochromator design has appeared very recently [12]. This novel design is based on the use of a toroidal grating, and adopts a constant entrance-angle mode of operation. The resolution and the photon energy range are the same, but the delay of the photons is about three times smaller. Therefore, the perturbations of the electron beam distributions generated in this way would be negligible.

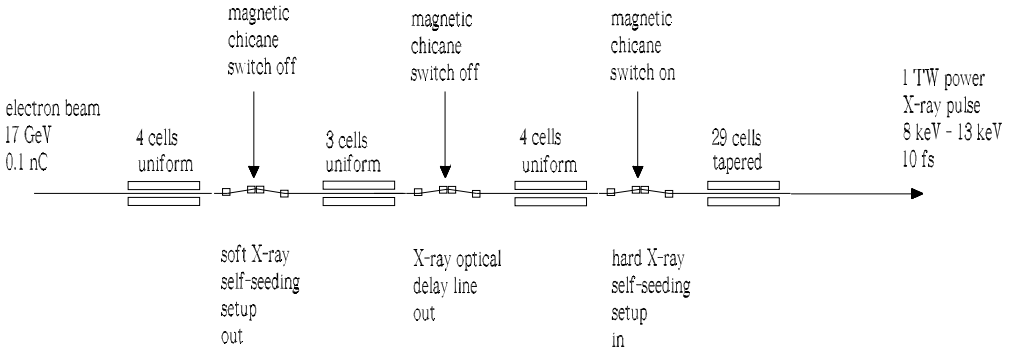

Fig. 12. Design of the undulator system for 1 TW power mode of operation in the 8 keV - 13 keV photon energy range. The method exploits a self-seeding scheme with crystal monochromator.

3.4 Generation of TW pulses in 8 keV - 13 keV energy range

Fig. 12 shows the basic setup for the high-power mode of operation in the hard X-ray photon energy range. The first and the second chicane are not used in this regime, and are switched off. After the first three undulators and the single-crystal monochromator, a fourth output-undulator follows. Under the constraints imposed by the undulator parameters it is possible to operate at two nominal electron beam energies of 14 GeV and 17.5 GeV. The setup was optimized based on results of the start-to-end simulations for an electron beam energy of 17.5 GeV and a nominal electron beam with 0.1 nC charge. Results are presented in section 4. The output undulator is long enough to reach 1 TW power. The duration of the output pulses is of about 10 fs. In this mode of operation there is no possibility to tune the pulse duration without changing the electron beam distribution. If tunability of the pulse duration is requested in this energy range, this is most easily achieved by providing additional delay with a magnetic chicane installed behind the hard X-ray self-seeding setup.

3.5 Location and expansion plans

The original design of the European XFEL [44] was optimized to produce XFEL radiation at 0.1 nm, simultaneously at two undulator lines, SASE1 and SASE2. Additionally, the design included one FEL line in the soft X-ray range, SASE3, and two undulator lines for spontaneous synchrotron radiation, U1 and U2, Fig. 13. The soft X-ray SASE3 beamline used the

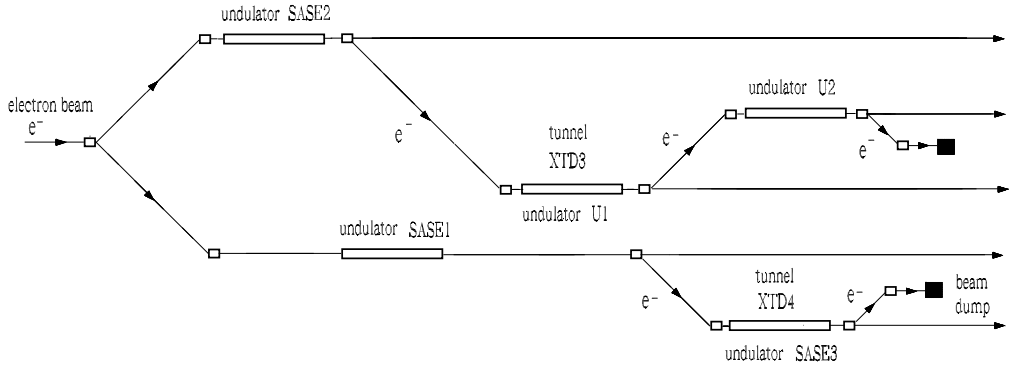

Fig. 13. Original design of the European XFEL facility.

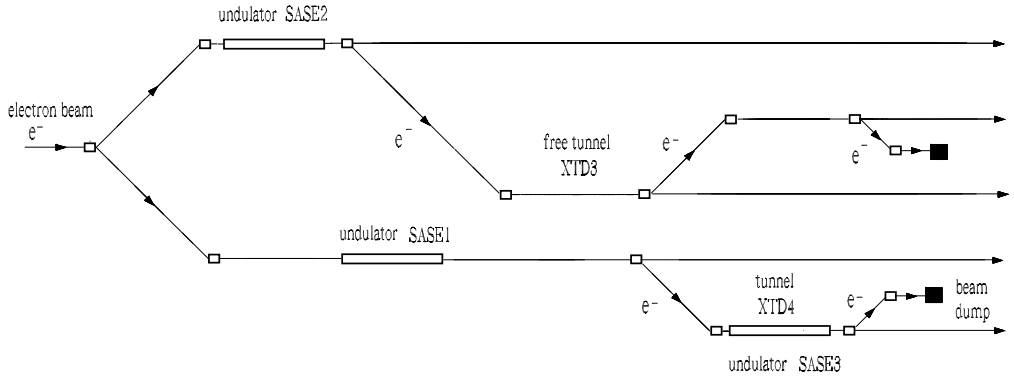

Fig. 14. Current design of the European XFEL facility.

spent electron beam from SASE1, and the U1 and U2 beamlines used the spent beam from SASE2. In fact, although the electron beam performance is degraded by the FEL process, the beam can still be used in afterburner mode in the SASE3 undulator, which will be equipped with a 126 m-long undulator system, for a total of 21 cells.

After a first design report, the layout of the European XFEL changed. In the last years after the achievement of the LCLS, and the subsequent growth of interest in XFEL radiation by the scientific community, it became clear that the experiments with XFEL radiation, rather than with spontaneous synchrotron radiation, had to be prioritized. In the new design, the two beamlines behind SASE2 are now free for future XFEL undulators installations, Fig. 14.

Recently it was also realized that the amplification process in the XFEL un-

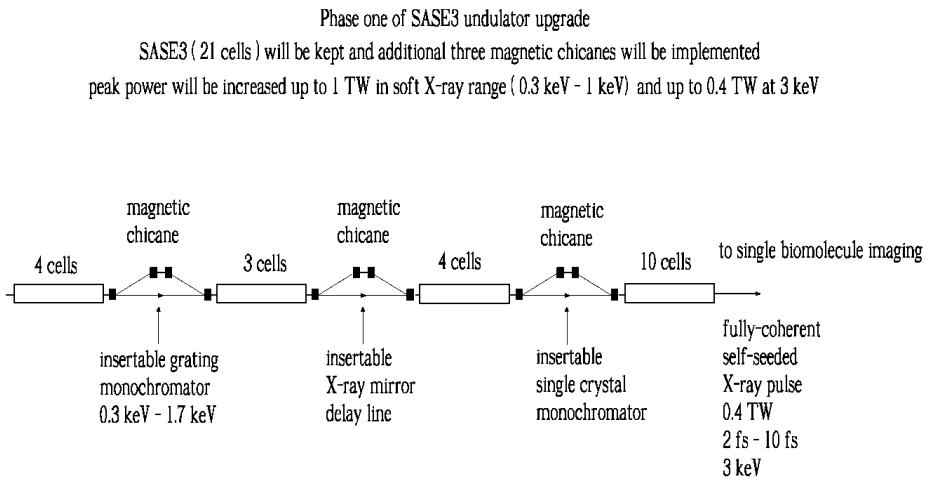

Fig. 15. Phase 1 of the SASE3 upgrade. Schematic layout of the SASE3 beamline after installation of three additional magnetic chicanes. Phase 1 experiments will aim to demonstrate the effectiveness of the combination of self-seeding, fresh bunch and undulator tapering techniques in the photon energy range between 3 keV and 5 keV, and to serve as a test bench before the installation of additional undulators (Phase 2). The Phase 1 upgrade will allow for single biomolecule imaging in the preferable photon energy range between 3 keV and 5 keV.

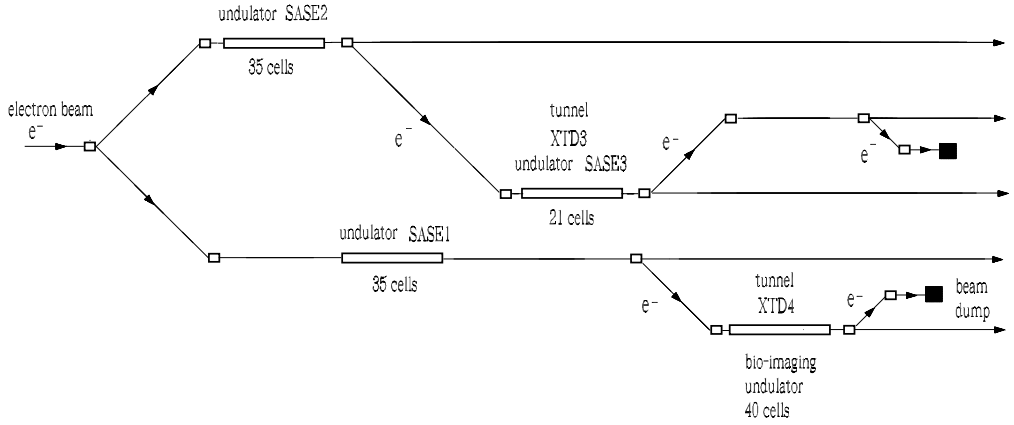

Fig. 16. Schematic of the proposed extension of the European XFEL facility.

dulators can be effectively controlled by betatron FEL switchers [41, 42]. The SASE3 undulator was then optimized for generating soft X-rays. However, due to the possibility of switching the FEL process in SASE1, it is possible to produce high power SASE3 radiation in a very wide photon energy range between 0.3 keV and 13 keV. The SASE3 beamline is now expected to provide excellent performance, and to take advantage of its location in the XTD4 tunnel, which is close to the experimental hall and has sufficient free space behind the undulator for future expansion (140 m). After this section, the electron beam will be separated from the photon beam and will

be bent down to an electron beam dump, Fig. 13. In the photon energy range between 3 keV and 13 keV, the SASE3 beamline is now expected to provide even better conditions for users than SASE1 and SASE2.

In this article we propose to build the bio-imaging beamline in the XTD4 tunnel as an upgrade of SASE3.

The first installation phase of the bio-imaging beamline described in this report includes the installation of the full SASE3 undulator system, constituted by 21 cells, together with three magnetic chicanes, after the 4th, the 7th and the 11th cell, Fig. 15. These three chicanes will be equipped with self-seeding setups in the soft X-ray (first chicane), in the hard X-ray (third chicane), and with an X-ray mirror delay line (second chicane). They constitute the most important elements of proposed bioimaging beamline design. The start of commissioning and operation of the entire beamline is defined by the completion of these elements. Our results (see section 4) suggest that 400 GW output power in the wavelength range between 3 keV and 5 keV is possible from the last tapered undulator part, consisting of 10 cells. The cost for soft X-ray self-seeding setup, fresh bunch technique setup and hard X-ray self-seeding setup can be estimated as 2 M EUR, 1 M EUR and 1 M EUR respectively. This installation phase will play a most important role in the construction of the new beamline.

After the experimental demonstration of self-seeding and fresh bunch techniques feasibility, a second installation phase will follow, including the extension of the line with additional 19 undulator cells for achieving 1 TW peak power in the entire photon energy range. The cost for one cell can be estimated as 0.5 M EUR [2]. This amounts to about 10 M EUR for the undulator extension.

In a possible third stage, a new SASE3 undulator composed by 21 cells can be installed in the free XTD3 tunnel, which is shorter than the XTD4 tunnel but sufficiently long for such installation, Fig. 16.

The bio-imaging beamline will support experiments carried out over a rather wide photon energy range. It is therefore proposed that the photon beam transport of the new beamline includes two lines. Line A uses 0.5m-long mirrors operating at a grazing angle of 2 mrad. This line is dedicated to the transport of X-ray radiation in the photon energy range from 3 keV up to 13 keV. This would be complementary to the designed SASE3 line, Line B, that is now optimized in the soft X-ray range between 0.3 keV and 3 keV. The distance from the 40-cells-long undulator exit to the first

[2] The cost of one undulator segment and intersection setup can be estimated as 0.3 M EUR and 0.13 M EUR, respectively.

Table 1
Undulator parameters

	Units	
Undulator period	mm	68
Periods per cell	-	73
K parameter (rms)	-	1.5-7
Total number of cells	-	40
Intersection length	m	1.1
Photon energy	keV	0.3-13

mirror system will be only of about 100m [3] .

4 FEL studies

With reference to Fig. 7, Fig. 8 and Fig. 12 we performed feasibility studies pertaining the three energy ranges considered in this articles. These studies were performed with the help of the FEL code GENESIS 1.3 [45] running on a parallel machine. Simulations are based on a statistical analysis consisting of 100 runs.

In order to specify the electron beam parameters for the simulations we use results from electron beam start-to-end simulations at the entrance of SASE3 [46]. In particular, Fig. 17 refers to the soft X-ray case, where the energy of the electron beam is 10.5 GeV, while Fig. 18 refers to the hard X-ray case, where the energy of the electron beam is 17.5 GeV. It should be remarked that the start-to-end simulations in [46] actually give back the beam parameters at the entrance of SASE1. Therefore, resistive wakefields up to the SASE3 entrance modify the electron beam energy. Moreover, here we assume that the lasing in SASE1 is inhibited with the help of the betatron switcher technique [41, 42], but that the undulator gap is not opened. Therefore, energy spread due to quantum fluctuations in SASE1 must be accounted for. We illustrated the change in both energy and energy spread due to these processes in Fig. 18, where two curves are present in the pictures in the second row. In the following simulations we will use the current profile the normalized emittance the energy profile the electron beam energy spread

[3] This is in contrast with SASE1 and SASE2 beamlines, where an opening angle of 0.003 mrad at 3 keV FEL radiation leads to unacceptable mirror length of 2 m due to long distance of about 500 m between the source and mirror system. For these beamlines there is no possibility to use identical configuration of mirrors within the photon energy range from 3 keV to 13 keV.

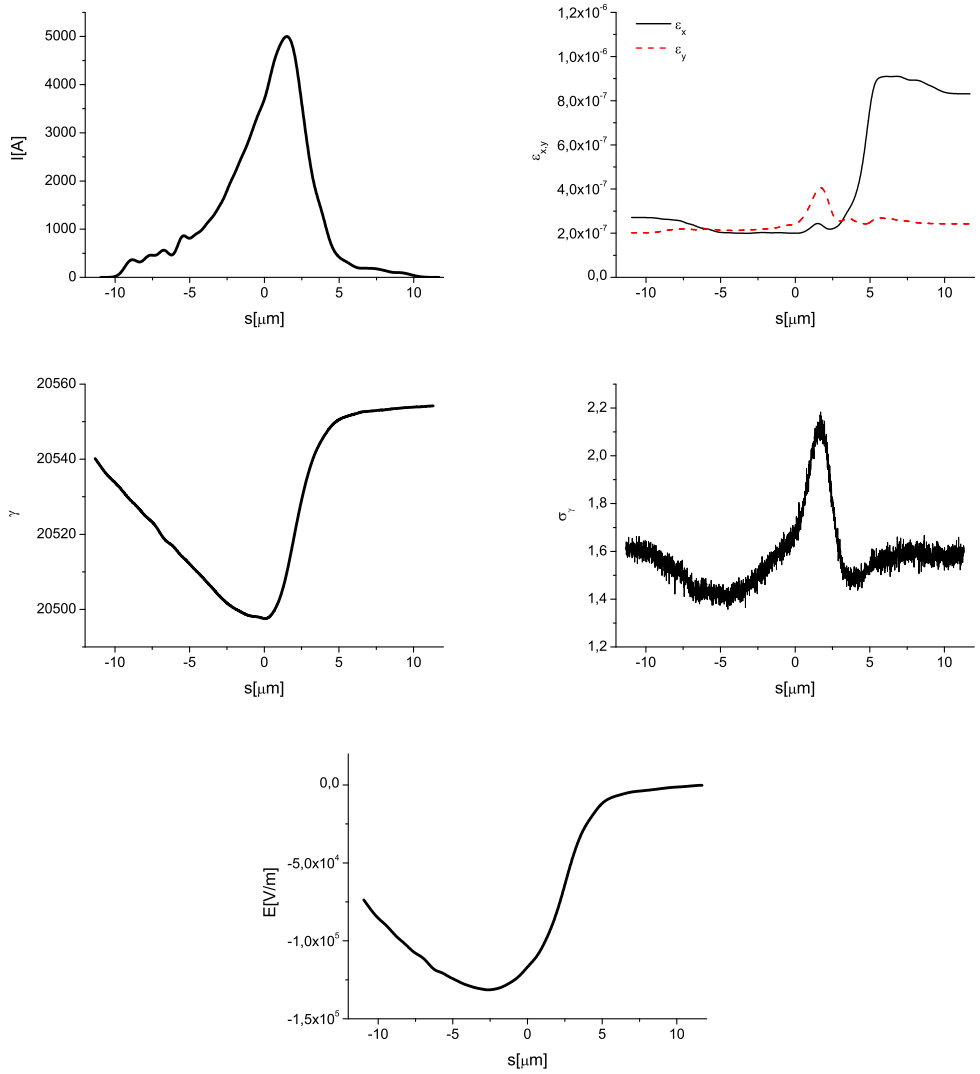

Fig. 17. Results from electron beam start-to-end simulations at the entrance of SASE3 [46] for the soft X-ray case. (First Row, Left) Current profile. (First Row, Right) Normalized emittance as a function of the position inside the electron beam. (Second Row, Left) Energy profile along the beam. (Second Row, Right) Electron beam energy spread profile. (Bottom row) Resistive wakefields in the SASE3 undulator [46]. These results are used as starting point for our investigations in the soft X-ray regime, Section 4.1 and 4.2.

and the resistive wakefields in the SASE3 undulator from Fig. 17 (Section 4.1 and 4.2) and from Fig. 18 (Section 4.3). The undulator parameters are presented in Table 1.

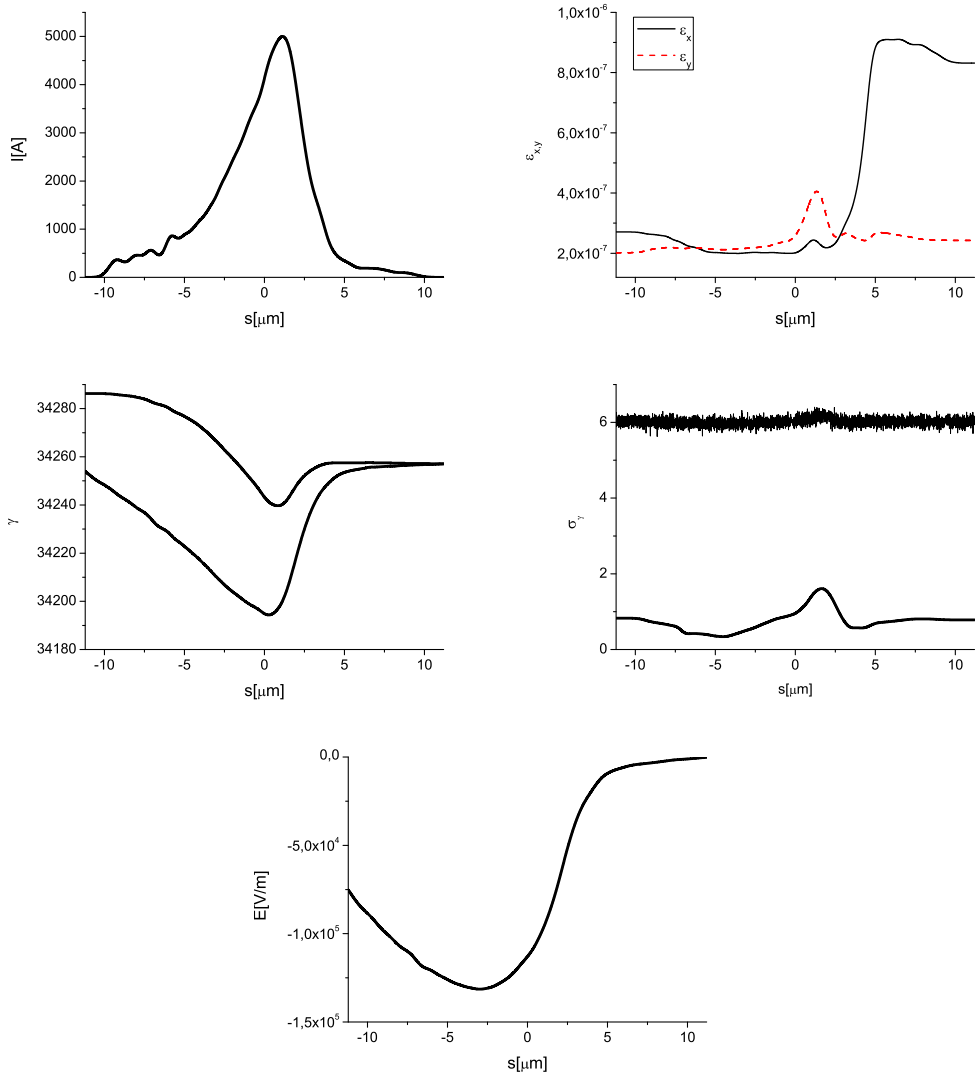

Fig. 18. Results from electron beam start-to-end simulations at the entrance of SASE3 [46] for the hard X-ray case. (First Row, Left) Current profile. (First Row, Right) Normalized emittance as a function of the position inside the electron beam. (Second Row, Left) Energy profile along the beam, lower curve. The effects of resistive wakefields along SASE1 are illustrated by the comparison with the upper curve, referring to the entrance of SASE1 (Second Row, Right) Electron beam energy spread profile, upper curve. The effects of quantum diffusion along SASE1 are illustrated by the comparison with the lower curve, referring to the entrance of SASE1. (Bottom row) Resistive wakefields in the SASE3 undulator [46]. These results are used as starting point for our investigations in the soft X-ray regime, Section 4.3.

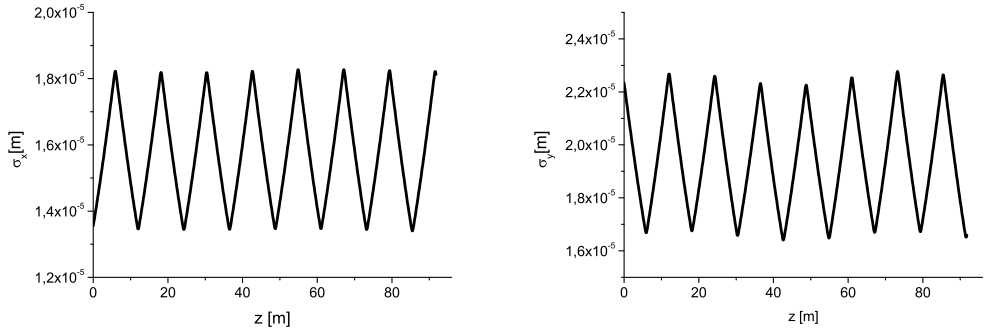

Fig. 19. Evolution of the horizontal (left plot) and vertical (right plot) dimensions of the electron bunch as a function of the distance inside the undulator at 10.5 GeV. The plots refer to the longitudinal position inside the bunch corresponding to the maximum current value.

4.1 Soft X-ray photon energy range below 1 *keV*

Production of soft X-rays with photon energies below 1 keV is enable by configuring the setup as described in Fig. 7, and discussed in Section 3.2. A feasibility study for this case has been already carried out in [40], to which we refer the reader for further details and simulation results.

4.2 Photon energy range between 3 *keV and* 5 *keV*

We now turn to analyze the case described in Fig. 8, which pertains the energy range between 3 keV and 5 keV.

The expected beam parameters at the entrance of the SASE3 undulator, and the resistive wake inside the undulator are shown in Fig. 17. The evolution of the transverse electron bunch dimensions are plotted in Fig. 19.

We begin our investigation by simulating the SASE power and spectrum after the first 4 undulator cells, that is before the first magnetic chicane. Results are shown in Fig. 20.

The magnetic chicane is switched on, an the soft X-ray monochromator is inserted. Assuming a monochromator efficiency of 10%, a Gaussian line, and a resolving power of 5000 we can filter the incoming radiation pulse in Fig. 20 accordingly, to obtain the power and spectrum in Fig. 21. This power and spectrum are used for seeding.

Since we now deal with a conventional grating monochromator, the photon pulse is delayed with respect to the electron pule. In our study case we

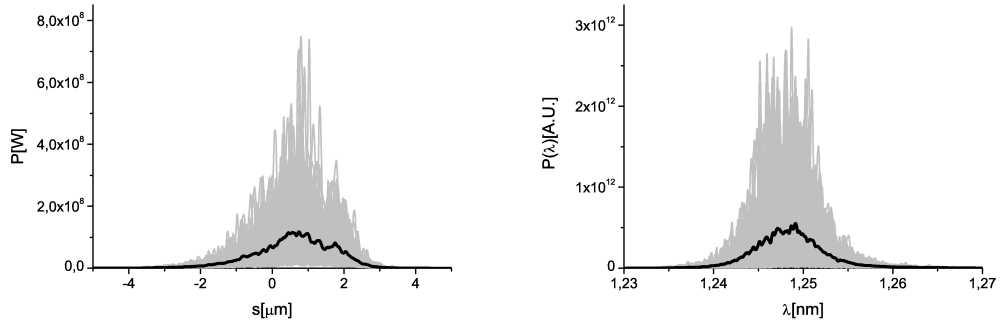

Fig. 20. Power and spectrum before the first magnetic chicane. Grey lines refer to single shot realizations, the black line refers to the average over a hundred realizations.

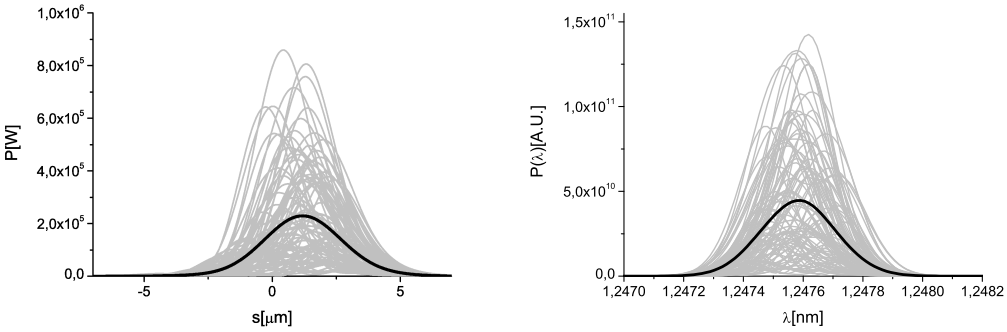

Fig. 21. Power and spectrum after the first magnetic chicane and soft X-ray monochromator. Grey lines refer to single shot realizations, the black line refers to the average over a hundred realizations.

assume a relatively large delay of about 3 ps. In order to compensate for such delay, one needs a chicane with a relatively large dispersion strength $R_{56} \sim 2$ mm. This assumption is conservative, and as the design efforts of the LCLS crew continue, a better monochromator design with shorter photon delay is likely to be designed, which will have positive effects on the design of the chicane. However, assuming for the time being $R_{56} = 2$ mm, we cannot neglect, in principle, the effects of the chicane dispersion on the electron bunch properties. We accounted for them with the help of the code Elegant [43], which was used to propagate the electron beam distribution through the chicane. Results are shown in Fig. 22.

Since the R_{56} is large enough to wash out the electron beam microbunching, we assume a fresh bunch, at the entrance of the following undulator part constituted by 3 undulator cells. This means that the results in Fig. 22 are taken to generate a new beam file to be fed into GENESIS. The electron bunch is now seeded with the monochromatized radiation pulse in Fig. 21, so that the seed is amplified in the 3 undulator cells following the chicane. After that, the electron beam is sent through the second chicane, while the

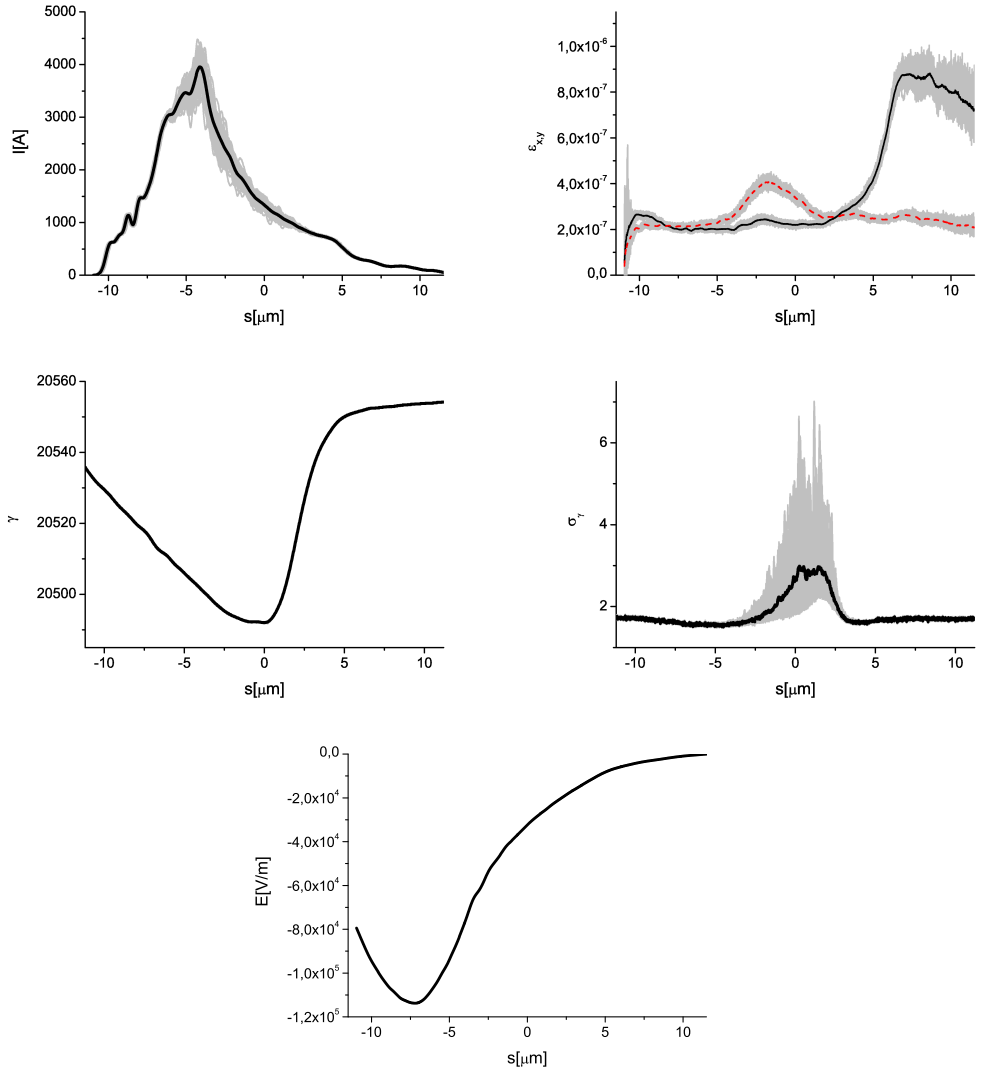

Fig. 22. Electron beam characteristics after the second magnetic chicane. (First Row, Left) Current profile. (First Row, Right) Normalized emittance as a function of the position inside the electron beam. (Second Row, Left) Energy profile along the beam. (Second Row, Right) Electron beam energy spread profile. (Bottom row) Resistive wakefields in the SASE3 undulator [46].

radiation pulse goes through the X-ray optical delay line described in Fig. 6, where the radiation pulse is delayed of about 6 fs with respect to the electron beam, as shown in Fig. 9. The power and spectrum of the radiation pulse after the optical delay line are shown in Fig. 24, where the effect of the optical delay is illustrated.

Besides allowing for the installation of the optical delay line, which delays the radiation pulse of about half of the electron bunch size, the second chicane also smears out the microbunching in the electron bunch. As a result, at the entrance of the third undulator part the electron bunch can

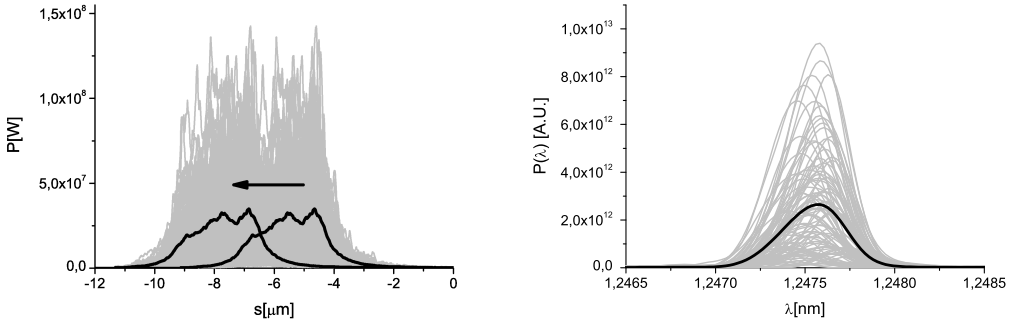

Fig. 23. Power and spectrum at the fundamental harmonic after the second chicane equipped with the X-ray optical delay line, delaying the radiation pulse with respect to the electron bunch. Grey lines refer to single shot realizations, the black line refers to the average over a hundred realizations.

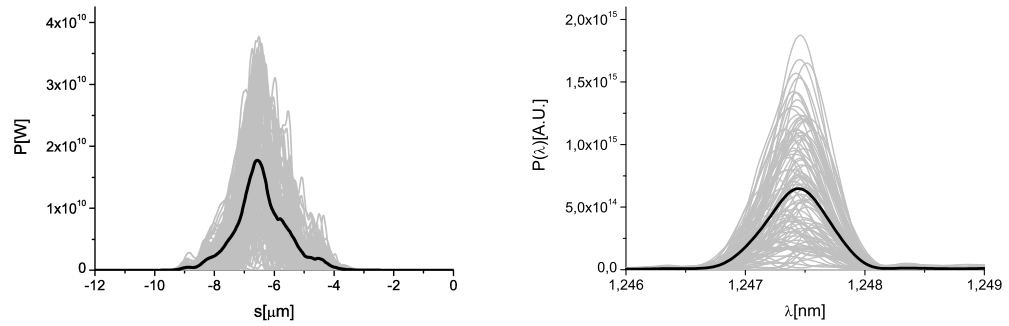

Fig. 24. Power and spectrum at the fundamental harmonic at the exit of the third undulator and before the third magnetic chicane. Grey lines refer to single shot realizations, the black line refers to the average over a hundred realizations.

be considered as unmodulated, and half of it is seeded with the radiation pulse. The seeded half of the electron bunch amplifies the seed in the third undulator part, composed by four cells. After that, electrons and radiation are separated once more going through the third chicane. The hard X-ray self-seeding crystal is out, and the chicane simply acts as a delay line for the electron beam, which also smears out the microbunching. Power and spectrum following the third chicane are shown in Fig. 24.

The seeded part of the electron bunch is now spent, and its quality has deteriorated too much for further lasing. However, by tuning the third chicane in the proper way, one can superimpose the radiation beam onto that part of the electron bunch that has not been seeded in the third undulator part. This is fresh, and can lase again in the fourth undulator part. The fourth undulator part is not tuned at the fundamental harmonic, but rather at the third harmonic. This allows to reach the photon energy range between 3 keV and 5 keV. In fact, the power at the third harmonic, shown in Fig. 25

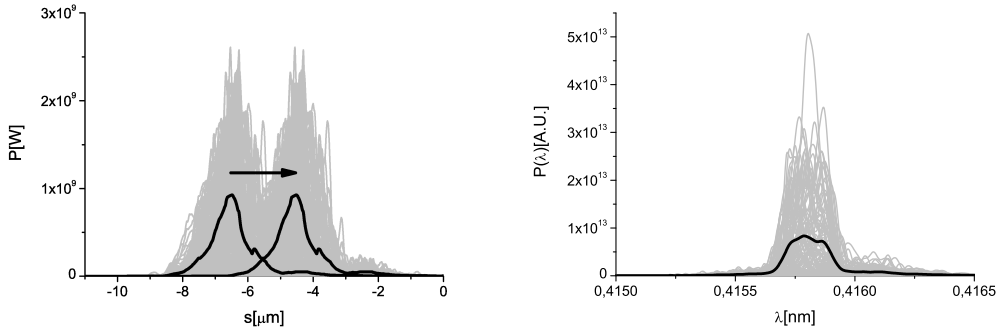

Fig. 25. Power and spectrum at the third harmonic after the third magnetic chicane. Grey lines refer to single shot realizations, the black line refers to the average over a hundred realizations.

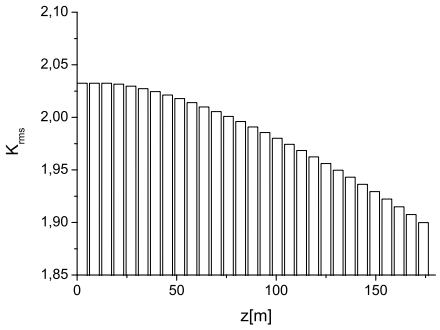

Fig. 26. Tapering law for the case $\lambda = 0.4$ nm.

together with the relevant spectrum, is sufficient to act as a seed in the last part of the undulator. Fig. 25 also shows the effect of the magnetic chicane, which delays the electron bunch relative to the radiation pulse in order to allow for the seeding of the fresh part of the bunch.

The fourth and last part of the undulator is composed by 29 cells, and is partly tapered, post-saturation, to allow for increasing the region where electrons and radiation interact properly to the advantage of the radiation pulse. Tapering is implemented by changing the K parameter of the undulator segment by segment according to Fig. 26. The tapering law used in this work has been implemented on an empirical basis.

The use of tapering together with monochromatic radiation is particularly effective, since the electron beam does not experience brisk changes of the ponderomotive potential during the slippage process. The final output is presented in Fig. 27 in terms of power and spectrum. As one can see, simulations indicate an output power of about 1 TW.

The energy of the radiation pulse and the energy variance are shown in Fig. 28 as a function of the position along the undulator. The divergence and

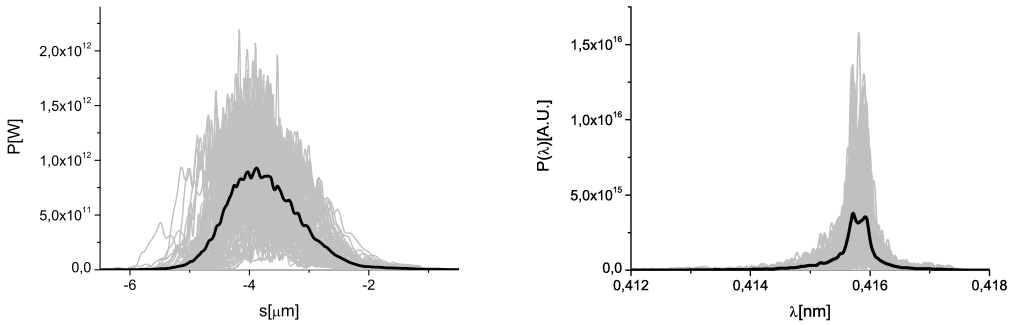

Fig. 27. Final output. Power and spectrum at the third harmonic after tapering. Grey lines refer to single shot realizations, the black line refers to the average over a hundred realizations.

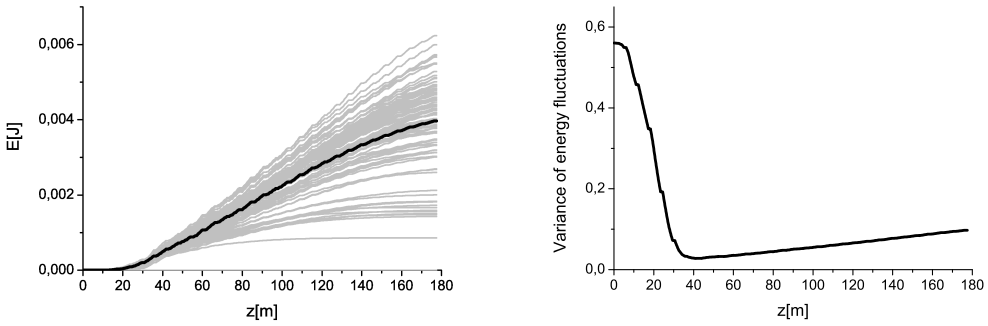

Fig. 28. Final output. Energy and energy variance of output pulses for the case $\lambda = 0.4$ nm. In the left plot, grey lines refer to single shot realizations, the black line refers to the average over a hundred realizations.

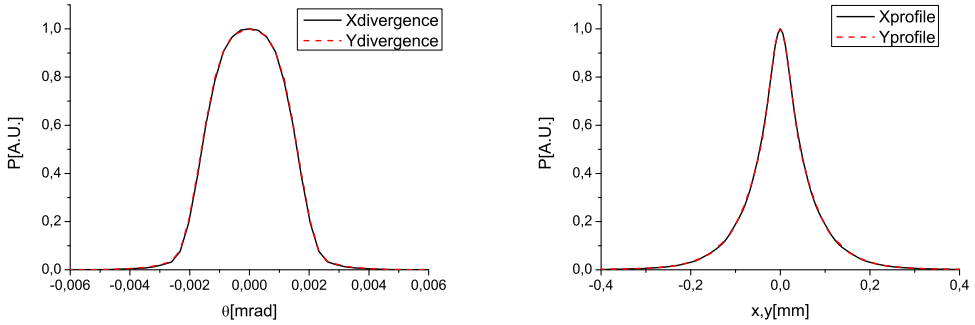

Fig. 29. Final output. X-ray radiation pulse energy distribution per unit surface and angular distribution of the X-ray pulse energy at the exit of output undulator for the case $\lambda = 0.4$ nm.

the size of the radiation pulse at the exit of the final undulator are shown, instead, in Fig. 29. In order to calculate the size, an average of the transverse intensity profiles is taken. In order to calculate the divergence, the spatial Fourier transform of the field is calculated.

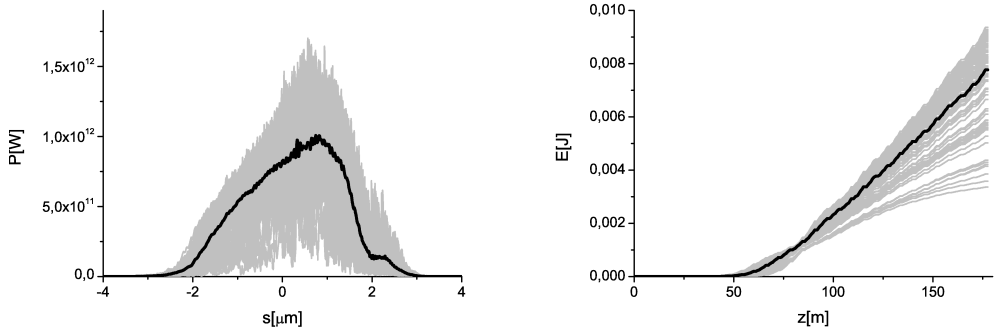

Fig. 30. Output radiation pulse obtained from simulations using unperturbed electron bunch parameters (small momentum compaction factor R_{56} of first chicane) for the case $\lambda = 0.4$ nm. They show (left) the temporal distribution of the output power and (right) the energy per pulse as a function of the undulator length. Note that the change in power and energy with respect to the case of perturbed electron bunch (where $R_{56} = 2$ mm), presented in Fig. 27 and Fig. 28, is relatively small. Grey lines refer to single shot realizations, the black line refers to the average over a hundred realizations.

Finally, it is interesting to discuss the effect of the relatively large value of the dispersion in the first chicane $R_{56} = 2$ mm. As one can see by comparing Fig. 17 and Fig. 22 the electron bunch characteristics changes in a seemingly non-negligible way. However, using unperturbed electron bunch parameters, that is assuming a negligible R_{56} an thus using Fig. 17 for generating the beam file after the soft X-ray self-seeding setup, results for the final power and energy in the pulse do not appreciably change. This can be seen by comparing Fig. 27 with Fig. 30, which is calculated in the limit for a negligible R_{56} in the first chicane. Small differences in the behaviors of power and energy are due to slightly different tuning of the simulation parameters.

4.3 Hard X-ray photon energy range above 8 keV

Finally, we consider the case described in Fig. 9, which pertains the hard X-ray energy above 8 keV.

The expected beam parameters at the entrance of the SASE3 undulator, and the resistive wake inside the undulator are shown in Fig. 18. The evolution of the transverse electron bunch dimensions are plotted in Fig. 31, where the varying quadrupole strength along the setup is also shown.

The first two magnetic chicanes are now switched off, and both the soft X-ray self-seeding setup and the X-ray optical delay line are out. Therefore, the electron beam lases in SASE mode along the first 11 undulator cells before passing through the single-crystal monochromator filter. The power

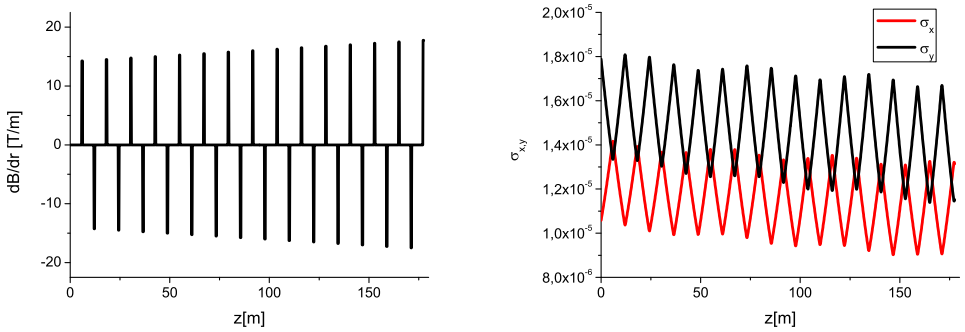

Fig. 31. Quadrupole strength (left) and electron beam size (right) as a function of the position inside the undulator at 17.5 GeV. The electron beam size refers to the longitudinal position inside the bunch corresponding to the maximum current value.

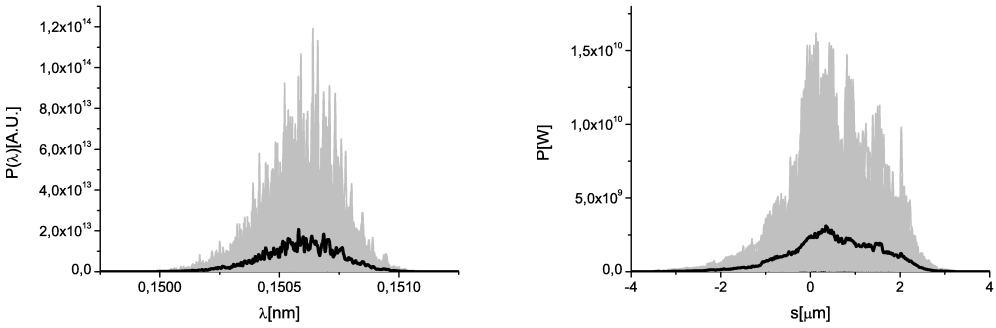

Fig. 32. Incident spectrum (left) and power (right) at the hard X-ray self-seeding crystal setup.

and the spectrum of the incident pulse are shown in Fig. 32. The difference with respect to a previously proposed hard X-ray self-seeding setup for the SASE1/2 lines (see [26]) is that in that case we were referring to a cascade self-seeding setup, which considerably increases the signal-to-noise ratio of the seeded signal compared to the SASE background. This allowed for a considerably smaller incident power level on the crystal (compare Fig. 32 with Fig. 13 of reference [26]). In the present case the setup should run at a repetition rate much smaller than in the case discussed in [26]. As a result, the heat loading on the crystal will be much less severe, and the requirement of a small incident power level on the crystal can be relaxed.

The effect of the filtering process is illustrated, both in the time and in the frequency domain, in Fig. 33. In the frequency domain the filter acts as a bandstop filter, effectively drilling a ”hole” in the spectrum of the incident signal. In the time domain, the outcoming pulse consists of the almost unperturbed incident pulse transmitted through the crystal, followed by a monochromatic tail of radiation, at much lower power level, which is due

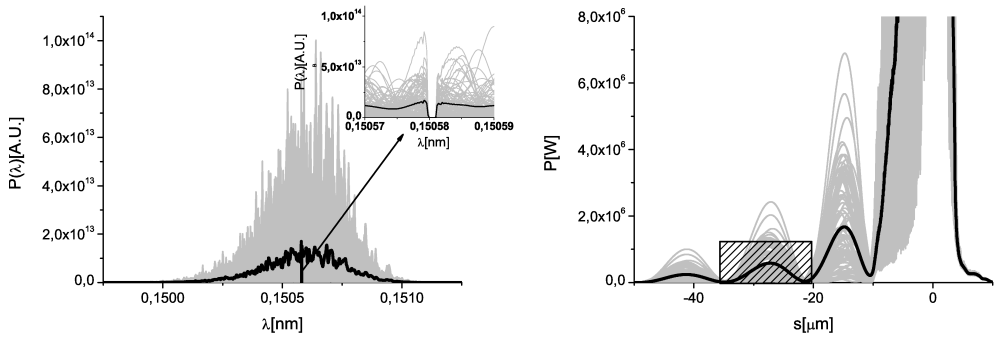

Fig. 33. Hard X-ray self-seeding mechanism in the frequency(left) and in the time domain (right). In the frequency domain the diamond crystal acts as a bandstop filter. Due to the presence of this filter, a monochromatic tail follows the SASE pulse in the time domain. The position of the electron bunch relative to such monochromatic tail can be controlled after the chicane is highlighted in the plot.

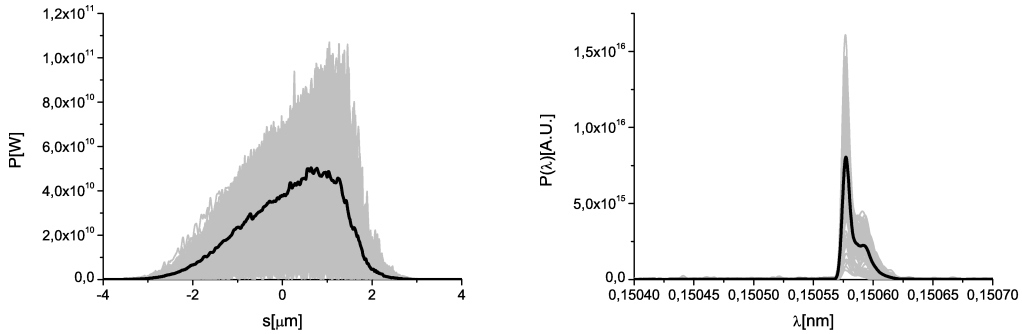

Fig. 34. Power and spectrum of output pulses at saturation. Grey lines refer to single shot realizations, the black line refers to the average over a hundred realizations.

to the presence of the crystal. The chicane is tuned in such a way that the electron bunch is superimposed onto the monochromatic tail, which now acts as seed.

The seed is amplified up to saturation in the output undulator. The power and the spectrum of the output pulse at saturation are shown in Fig. 34, while the energy and the energy variance as a function of the undulator length are plotted in Fig. 35. Saturation is reached after 11 segments.

As already discussed, we can use post-saturation tapering to increase the output power level. The tapering configuration in Fig. 36 is optimized for maximum output power level. Note that in this case tapering begins already after 10 segments, while the previously treated case with no tapering indicates that the optimal output is reached after 11 segments.

The output characteristics, in terms of power and spectrum, are shown in Fig. 37. The output power is increased of about a factor 20, allowing one

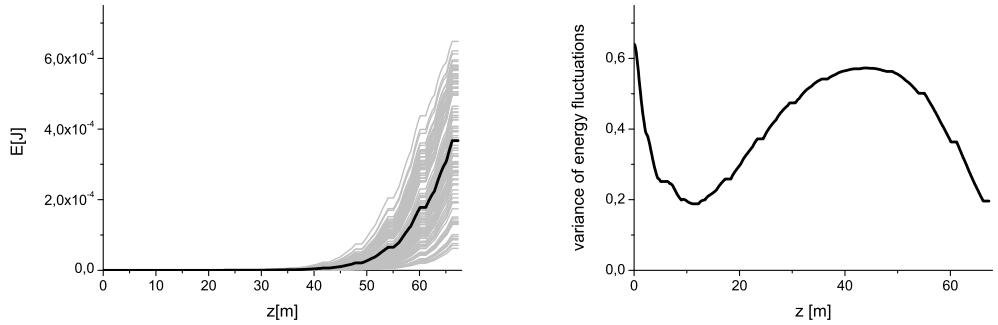

Fig. 35. Energy and energy variance of output pulses at saturation for the case $\lambda = 0.15$ nm. In the left plot, grey lines refer to single shot realizations, the black line refers to the average over a hundred realizations.

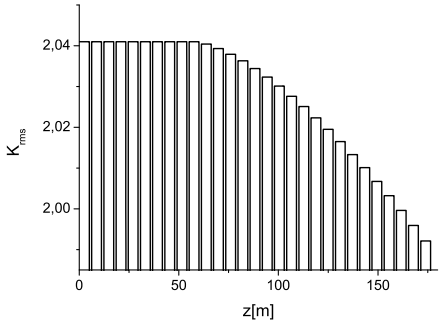

Fig. 36. Tapering law for the case $\lambda = 0.15$ nm.

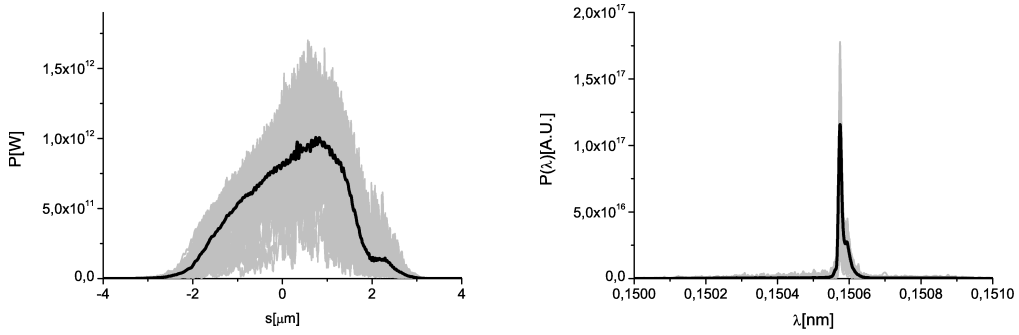

Fig. 37. Final output in the case of tapered output undulator for $\lambda = 0.15$ nm. Power and spectrum are shown. Grey lines refer to single shot realizations, the black line refers to the average over a hundred realizations.

to reach about one TW. The spectral width remains almost unvaried. The output level has been optimized by changing the tapering law, resulting in Fig. 36, and by changing the electron beam transverse size along the undulator, as suggested in [39], and shown in Fig. 31. Optimization was performed empirically. The evolution of the energy per pulse and of the

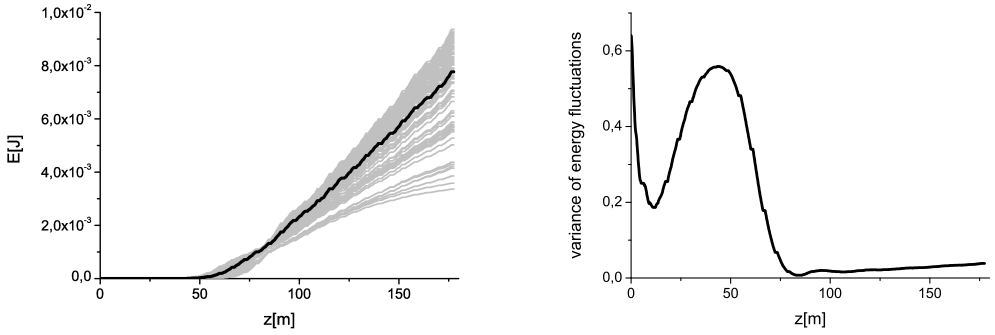

Fig. 38. Energy and energy variance of output pulses in the case of tapered output undulator for $\lambda = 0.15$ nm. In the left plot, grey lines refer to single shot realizations, the black line refers to the average over a hundred realizations.

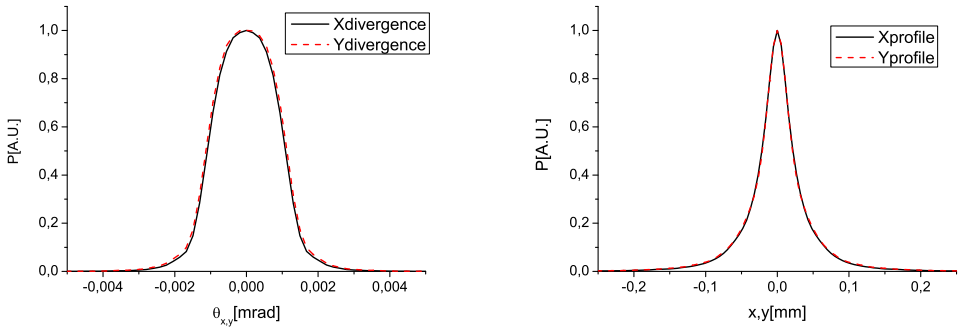

Fig. 39. Final output. X-ray radiation pulse energy distribution per unit surface and angular distribution of the X-ray pulse energy at the exit of output undulator for the case $\lambda = 0.15$ nm.

energy fluctuations as a function of the undulator length are shown in Fig. 38. Finally, the transverse radiation distribution and divergence at the exit of the output undulator are shown in Fig. 39.

5 Conclusions

This article describes a proposal for building a beamline dedicated to biomolecular imaging at the European XFEL. The present layout of the European XFEL enables to accommodate such extension. The final configuration foresees the new beamline located in the XTD4 tunnel, which is now occupied by SASE3, while the SASE3 beamline can be reinstalled inside the free XTD3 tunnel occupying the place instead of the previously planned spontaneous emission undulator U1. This final configuarion can be reached in two phases. During the low cost first phase, a soft X-ray self-seeding, a hard X-ray self-seeding and a fresh bunch setup will be implemented at the SASE3

beamline in XTD4. Initially, the SASE3 undulator (21 cells) can be kept as is, and three additional magnetic chicanes respectively equipped with grating monochromator, X-ray mirror delay line and crystal monochromator will be installed as soon as possible. This first phase constitutes a feasibility study of the system concept. Phase 1 experiments aim to demonstrate the combination of self-seeding, fresh bunch and undulator tapering techniques at photon energy range between 3 keV and 5 keV, and involve detailed benchmarking of simulations, in order to provide confidence in extrapolating results to higher power, that is to longer undulator length. During Phase 1, the peak power will be increased up to 1 TW in the soft X-ray range and up to 0.4 TW at operation energies around 3 keV. This upgrade of the SASE3 beamline will fundamentally improve the conditions for bio-imaging experiments. In particular, the concept of Phase 1 upgrade permits single protein molecule structure analysis in the most preferable photon energy range between 3 keV and 5 keV. However, during Phase 1, the maximum peak power in the hard X-ray range will still be smaller than 0.1 TW. In order to obtain 1 TW power in the photon energy range between 8 keV and 13 keV the installation of additional 19 undulator cells is necessary, Phase 2. With this installation the bio-imaging beamline will be optimized from the water window (0.3 keV) to K-edge of Selenium (13 keV) and the power will be increased to 1 TW in the entire photon energy range. In a final step, a beamline identical to SASE3 can be restored in XTD3.

The proposed upgrade program gives the possibility to build a beamline optimized for life science maintaining a world-leading position of the European XFEL in this field, by focusing experimental activities on studies taking advantage of single biomolecule imaging.

6 Acknowledgements

We are grateful to Massimo Altarelli, Reinhard Brinkmann, Henry Chapman, Janos Haidu, Viktor Lamzin, Serguei Molodtsov and Edgar Weckert for their support and their interest during the compilation of this work.

References

[1] J. Drenth, Principles of Protein X-ray Crystallography, third ed., Springer Science, LLC, New York, 2007

[2] B. Rupp, Biomolecular Crystallography, Garland Science, New York, 2010

[3] J. Hajdu, Curr. Opin. Struct. Biol. 10, 569 (2000) 2. R. Neutze et al.,

Nature 406, 752 (2000) 3. K. J. Gaffney and H. N. Chapman, Science 316, 1444 (2007)
[4] J. Fineup, Opt. Lett. 3, 27-29 (1978)
[5] R. Neutze et al., Nature 406, 752 (2000)
[6] M. M. Seibert et al., Nature 470 (7332) 78-81 (2011)
[7] The Protein Data Bank at http://www.rcsb.org/pdb/home/home.do
[8] J. Hajdu, Private Communication
[9] S. Ikeda and H. Kono, Optics Express v. 20, 3375 (2012)
[10] Y. Feng, J. Hastings, P. Heimann, M. Rowen, J. Krzywinski, and J. Wu, "X-ray Optics for soft X-ray self-seeding the LCLS-II", proceedings of 2010 FEL conference, Malmo, Sweden, (2010).
[11] Y. Feng, P. Heimann, J. Wu, J. Krzywinski, M. Rowen, and J. Hastings, "Compact Grating Monochromator Design for LCLS-I Soft X-ray Self-Seeding", https://slacportal.slac.stanford.edu/sites/lcls_public/lcls_ii/Lists/LCLS_II_Calendar/Physics_Meetings.aspx, May 2011 and https://sites.google.com/a/lbl.gov/realizing-the-potential-of-seeded-fels-in-the-soft-x-ray-regime-workshop/talks, October 2011
[12] D. Cocco, Private Communication.
[13] D. Cocco , A. Bianco , B. Kaulich , F. Schaefers , M. Mertin , G. Reichardt , B. Nelles, K. F. Heidemann "From Soft to Hard X-ray with a Single Grating Monochromator", AIP conference proceeding 879 (2006)
[14] J. Feldhaus et al., Optics. Comm. 140, 341 (1997).
[15] E. Saldin, E. Schneidmiller, Yu. Shvyd'ko and M. Yurkov, NIM A 475 357 (2001).
[16] E. Saldin, E. Schneidmiller and M. Yurkov, NIM A 445 178 (2000).
[17] R. Treusch, W. Brefeld, J. Feldhaus and U Hahn, Ann. report 2001 "The seeding project for the FEL in TTF phase II" (2001).
[18] A. Marinelli et al., Comparison of HGHG and Self Seeded Scheme for the Production of Narrow Bandwidth FEL Radiation, Proceedings of FEL 2008, MOPPH009, Gyeongju (2008).
[19] G. Geloni, V. Kocharyan and E. Saldin, "Scheme for generation of highly monochromatic X-rays from a baseline XFEL undulator", DESY 10-033 (2010).
[20] Y. Ding, Z. Huang and R. Ruth, Phys.Rev.ST Accel.Beams, vol. 13, p. 060703 (2010).
[21] G. Geloni, V. Kocharyan and E. Saldin, "A simple method for controlling the line width of SASE X-ray FELs", DESY 10-053 (2010).
[22] G. Geloni, V. Kocharyan and E. Saldin, "A Cascade self-seeding scheme with wake monochromator for narrow-bandwidth X-ray FELs", DESY 10-080 (2010).
[23] Geloni, G., Kocharyan, V., and Saldin, E., "Cost-effective way to enhance the capabilities of the LCLS baseline", DESY 10-133 (2010).
[24] J. Wu et al., "Staged self-seeding scheme for narrow bandwidth , ultrashort X-ray harmonic generation free electron laser at LCLS", proceed-

ings of 2010 FEL conference, Malmo, Sweden, (2010).
[25] G. Geloni, V. Kocharyan and E. Saldin, "Scheme for generation of fully coherent, TW power level hard x-ray pulses from baseline undulators at the European XFEL", DESY 10-108 (2010).
[26] Geloni, G., Kocharyan, V., and Saldin, E., "Production of transform-limited X-ray pulses through self-seeding at the European X-ray FEL", DESY 11-165 (2011).
[27] Geloni, G., Kocharyan V., and Saldin, E., "A novel Self-seeding scheme for hard X-ray FELs", Journal of Modern Optics, vol. 58, issue 16, pp. 1391-1403, DOI:10.1080/09500340.2011.586473 (2011)
[28] I Ben-Zvi and L. H. Yu, Nucl. Instr. and Methods, A 393, 96 (1997).
[29] W.M. Fawley et al., Toward TW-level LCLS radiation pulses, TUOA4, to appear in the FEL 2011 Conference proceedings, Shanghai, China, 2011
[30] J. Wu et al., Simulation of the Hard X-ray Self-seeding FEL at LCLS, MOPB09, to appear in the FEL 2011 Conference proceedings, Shanghai, China, 2011
[31] P. Emma et al., Nature photonics doi:10.1038/nphoton.2010.176 (2010)
[32] A. Lin and J.M. Dawson, Phys. Rev. Lett. 42 2172 (1986)
[33] P. Sprangle, C.M. Tang and W.M. Manheimer, Phys. Rev. Lett. 43 1932 (1979)
[34] N.M. Kroll, P. Morton and M.N. Rosenbluth, IEEE J. Quantum Electron., QE-17, 1436 (1981)
[35] T.J. Orzechovski et al., Phys. Rev. Lett. 57, 2172 (1986)
[36] W. Fawley et al., NIM A 483 (2002) p 537
[37] M. Cornacchia et al., J. Synchrotron rad. (2004) 11, 227-238
[38] X. Wang et al., PRL 103, 154801 (2009)
[39] Y. Jiao et al. Phys. Rev. ST Accel. Beams 15, 050704 (2012)
[40] Geloni, G., Kocharyan, V., and Saldin, E., "Self-seeding scheme for the soft X-ray line at the European XFEL", DESY 12-034 (2012).
[41] R. Brinkmann, E. Schnedmiller and M. Yurkov, DESY 10-011(2010) and
[42] F. J. Decker, et al., Multiple FELs from the one LCLS Undulator, THPB31, Proceedings of the 33rd FEL conference, Shanghai, China, 2011 to be published.
[43] M. Borland, http://www.aps.anl.gov/ Accelerator_Systems _Division/Accelerator_Operations _Physics/software.shtml#elegant
[44] M. Altarelli, et al. (Eds.) XFEL, The European X-ray Free-Electron Laser, Technical Design Report, DESY 2006-097, Hamburg (2006).
[45] S Reiche et al., Nucl. Instr. and Meth. A 429, 243 (1999).
[46] I. Zagorodnov, "Beam Dynamics Simulations for XFEL", http://www.desy.de/xfel-beam/s2e (2011).